Improved Low Voltage Ride-Through Capability of DFIG with ESO Controller under Unbalanced Network Conditions

Ali Akbar Vali[1*], Seyed Mohammad Hassan Hosseini[2], Javad Olamaei[3]
1- Department of Electrical Engineering, South Tehran Branch, Islamic Azad University, Tehran, Iran.
Email: aliakbarvali@yahoo.com (Corresponding author)
2- Department of Electrical Engineering, South Tehran Branch, Islamic Azad University, Tehran, Iran.
Email: Smhh110@azad.ac.ir
3- Department of Electrical Engineering, South Tehran Branch, Islamic Azad University, Tehran, Iran.
Email: J_olamaei@azad.ac.ir

Received: June 2020 Revised: August 2020 Accepted: October 2020

ABSTRACT:
Under unbalanced grid condition, in a Doubly-Fed Induction Generator (DFIG), voltage, current, and flux of the stator become asymmetric. Therefore, active-reactive power and torque will be oscillating. In DFIG controlling Rotor Side Converter (RSC) aims to eliminate power and torque oscillations. However, simultaneous elimination of the power and torque oscillations is not possible. Also, Grid Side Converter (GSC) aims to regulate DC-Link voltage. In this paper, in order to regulate DC-Link voltage, an Extended State Observer (ESO) based on a Generalized Proportional-Integral (GPI) controller, is employed. In this controlling method, DC-Link voltage is controlled without measuring the GSC current, and due to using the GPI controller, the improved dynamic response is resistant against voltage changes, and the settling time is reduced. To improve the transient stability and Low Voltage Fault Ride Through (LVRT) capability of DFIG, Statistic Fault Current Limiter (S-FCL) and Magnetic Energy Storage Fault Current Limiter (MES-FCL) are proposed in this paper. The proposed FCL does not only limit the fault current but also fasten voltage recovery. The simulations are implemented by MATLAB software in the synchronous positive and negative sequence reference (d-q).

KEYWORDS: DFIG, RSC, GSC, ESO, LVRT, FCL, Unbalanced grid.

1. INTRODUCTION

Dynamic Modeling and Control of Doubly-Fed Induction Generator (DFIG)-based wind generation system operating during unbalanced grid conditions were studied in [1], [2]. In a DFIG under unbalanced grid condition, voltage, current, and flux of the stator become asymmetric. If voltage unbalance is not taken into account by the control system, the stator current could be highly unbalanced even with a small unbalanced stator voltage [3]. Under unbalance grid conditions, the negative sequence component of stator voltage leads to the oscillation of power (active-reactive) and electromagnetic torque with twice the grid frequency. Power fluctuations lead to increased temperature in the stator winding, and torque fluctuations lead to mechanical tension on the rotor [4]. Control methods of DFIG are done based on the Voltage Orientation Control (VOC) or Flux Orientation Control (FOC). In the VOC method, the current signal controls the active power and along with the direct axis (Id) and reactive power along with the quadrature axis (Iq), and in the FOC method is conversely [5]-[7]. Control of DFIG for eliminating power and torque oscillation under unbalanced grid voltage was studied in [8]. In DFIG controlling Rotor Side Converter (RSC) aims to eliminate power and torque oscillations. However, simultaneous elimination of the stator active/reactive power and torque oscillations is not possible [9]. For the purpose of controlling the power and torque by RSC, multiple controller methods have been used. In [10], a sliding mode controller with fractional order sliding surface (SMC-F) based on robust control designed for controlling the performance of DFIG's RSC is used. In this control method to compensate uncertainties and incoming disturbances to the system, a sliding mode controller has been used. In order to increase the degree of freedom and further robustness of the

Paper type: Research paper
DOI: https://doi.org/10.29252/mjee.15.1.53
How to cite this paper: A. Akbar Vali, S. M. H. Hosseini, and J. Olamaei, "**Improved Low Voltage Ride-Through Capability of DFIG with ESO Controller under Unbalanced Network Conditions",** Majlesi Journal of Electrical Engineering, Vol. 15, No. 1, pp. 53-69. 2021.

controller, the sliding surface is selected as a fractional order form. In addition to increasing the performance of the controller, using a robust sliding mode controller causes a reduction to the chattering phenomenon in the input control signal. In [11], for the performance controlling of DFIG's RSC nonlinear robust control approach, an extended state observer based on the backstopping controller (ESO-BS) has been used. In this controller, the approach has a simple design and small computational complexity, which can eliminate nonlinear factors, as a result, computation complexity is reduced.

This paper aims to make the steady-state error value zero and improve the accuracy of controlling the RSC, Proportional-Integral (PI) controller is used. Under unbalanced grid conditions, common DC-link voltage is controlled by a Grid Side Converter (GSC). In order to control the DC-link voltage, multiple control methods have been used. In [12], to control the DC-Link voltage, the (FUZZY-PI) controller has been used. Complexity in performance and analysis is one of the most important disadvantages of this controller. In [13], to control DC-Link voltage, a nonlinear observer controller based on sliding mode control has been used. This controller has a suitable performance in controlling the DC-Link voltage, but it is slightly complicated in terms of analysis and regulation.

To solve this problem, in [14] a nonlinear observer controller based on high order sliding mode control has been used. This controller has a high sensitivity to a variety of disturbances and uncertainties. In [15]-[18], to control the DC-Link voltage, one cycle controller has been used. In this controller, the dynamic response is improved, and it is resistant to voltage changes, but it is complex in terms of the optimization of responses. In this paper, for controlling the DC-Link voltage, an Expanded State Observer (ESO) based on a Generalized Proportional-Integral (GPI) controller is introduced. In this controller, due to using the GPI controller, the improved dynamic response is resistant against voltage changes, and settling time is reduced [19]-[22]. In recent years, there have been numerous researches about enhancing Low Voltage Ride-Through (LVRT) capability of DFIG. In general, such methods can be divided into two categories: control-based solutions and hardware-based solutions that some of them are briefly reviewed in the following:

A. Control-based solutions

In [23], a genetic algorithm based LVRT control strategy is presented. A fault detection and confrontation control system is added to the previous control strategy, resulting in an improved LVRT control. In [24], an enhanced field-oriented control (EFOC) technique was adopted in the RSC of DFIG to improve power flow transfer and dynamic and transient stability. Proposed solution mitigates voltage sag and limits surge currents to enhance the operation of DFIG during symmetrical and asymmetrical faults. Researchers in [25] extend the studies of the DFIG behavior analysis during asymmetrical voltage sags using a frequency-domain modeling. A modified resonant controller is proposed to improve the system response during voltage sags, and the analysis of the Ride-Through Fault Capability (RTFC) based on the converter limits is carried out.

B. Hardware-based solutions

A conventional method to protect DFIG against high rotor currents during the grid faults and improve its LVRT behavior is implementation of the crowbar. This device consists of a bank of resistors connected to the rotor windings through power electronic devices. The major disadvantage of crowbar protection is that the RSC has to be disabled when the crowbar is active and hence, the generator consumes reactive power, leading to deterioration of the grid voltage [26] and power quality and reliability problems. Implementation of the Superconducting Fault Current Limiters (SFCLs) to enhance power system operation during faults is a proved fact [27]-[31]. Also SFCLs are suggested in some articles to improve LVRT behavior of DFIG wind turbines [12]-[14], but SFCL types and implementation methods are different. In [32], a superconducting fault current limiter is installed in the grid to improve FRT capability of DFIG. In [33], a switch-type FCL structure installed in series with the stator is described to enhance LVRT capability of DFIG. Moreover, a bridge-type FCL is introduced in [34] in the same location and its influence on DFIG LVRT is evaluated. In [35], three flexible AC transmission system (FACTS) devices are introduced to improve LVRT capability of fixed-speed wind farms. Proposed devices are the Gate-Controlled Series Capacitor (GCSC), the Thyristor Controlled Series Capacitor (TCSC) and Series Braking Resistor (SBR). Researchers prove the superiority of GCSC in comparison with two other devices, because it requires less power rating to stabilize the wind generator system. According to the modern grid codes, it is obligatory for the wind generator systems to remain operational during voltage disturbances, up to specified time periods and associated voltage levels. Grid code requirements for the wind power integration in Europe are well described in [36]. According to the German code, wind turbines connected to the power network have to sustain the operation within the 150 ms after the fault appearance, even if the voltage at the point of common coupling (PCC) falls to zero [37]. In this paper, the US grid code has been considered for analyzing the voltage stability during faults as

described by [38]. In this paper to enhance LVRT, two strategy of FCL are recommended. Statistic Fault Current Limiter (S-FCL) and Magnetic Energy Storage Fault Current Limiter (MES-FCL) are proposed. Using the proposed FCL, a balance is created between electrical and mechanical quantities. Therefore, the rotor speed deviation, electromagnetic torque fluctuations and requiring reactive power are reduced and LVRT capability of DFIG is improved.

2. DYNAMIC MODEL OF DFIG

The existing DFIG models are primarily developed on the basis of balanced grid conditions. Under unbalanced grid conditions, both positive and negative sequence components of voltage and current need to be considered in order to accurately describe the system behavior. With the purpose of obtaining a decoupled control between torque/active power and reactive power, the d-axis in the synchronous reference frame is generally oriented along the stator flux vector or the stator voltage vector. The equivalent circuit of a DFIG can be expressed in different reference frames such as the stationary frame, the rotor frame, or the synchronous frame fixed to either the stator voltage or the stator flux. A general expression of a DFIG model in an arbitrary (d-q) reference frame rotating at the angular speed of ω_s is shown in "Fig. 1". The stator and rotor flux are given, respectively, by:

$$\Psi_s=L_s i_s+L_m i_r \ , \ \Psi_r=L_r i_r+L_m i_s \tag{1}$$

From "Fig. 1", the stator and rotor voltages in the arbitrary reference frame can be expressed, respectively, as:

$$V_s=R_s i_s+\frac{d}{dt}\psi_s+j\omega_s\psi_s \tag{2}$$

$$V_r=R_r i_r+\frac{d}{dt}\psi_r+j(\omega_s-\omega_r)\psi_r \tag{3}$$

According to (1), the rotor flux and stator current can be expressed, respectively, as:

$$\psi_r=\frac{L_m}{L_s}\psi_s+\sigma L_r i_r \ , \ i_s=\frac{1}{L_s}(\psi_s-L_m i_r) \tag{4}$$

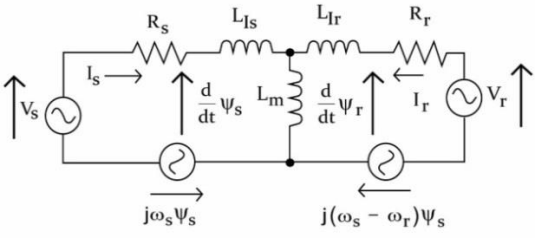

Fig. 1. DFIG model in (d-q) reference frame

Substituting (4) into (3) yields the rotor voltage in the arbitrary rotating reference frame as:

$$V_r=R_r i_r+\sigma L_r\frac{d}{dt}i_r+\frac{L_m}{L_s}\frac{d}{dt}\psi_s+j(\omega_{slip})(\sigma L_r i_r+\frac{L_m}{L_s}\psi s) \tag{5}$$

Where $\sigma=1-\frac{L_m^2}{L_s L_r}$ is the leakage factor. In (1) to (5), V_s, V_r are terminal voltages of stator and rotor, i_s , i_r are output currents of stator and rotor, ψ_s, ψ_r are leakage flux of stator and rotor, R_s, R_r are the resistance of stator and rotor, L_s, L_r are inductance of stator and rotor and L_m is magnetizing inductance, ω_s, are ω_{slip}, ω_r synchronous speed of stator, rotor speed, and slip frequency, respectively [1]-[4].

2.1. Balanced Grid Conditions*:*

In numerous articles, a detailed model of the DFIG system under a balanced network supply has been studied. Thus, only a brief description is given here. "Fig. 2" shows the phasor diagram of the variable F, which represents voltage, current, or flux, in the stator flux oriented (d-q), stator $(\alpha\text{-}\beta)$, and rotor $(\alpha_r\text{-}\beta_r)$ reference frames. The transformation between (dq), $(\alpha\text{-}\beta)$ and $(\alpha_r\text{-}\beta_r)$ reference frames are given by:

$$F_{dq}=F_{\alpha\beta}e^{-j(\omega_s t)}, F_{\alpha\beta}=F_{\alpha r\beta r}e^{j(\omega_r t)} \tag{6}$$

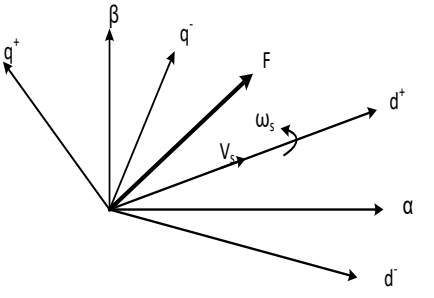

Fig. 2. Diagram of positive (dq^+) and negative (dq^-)

In balanced grid conditions, stator voltage is usually constant, which results in constant stator flux, relationship (5) can be expressed as:

$$V_r=R_r i_r+\sigma L_r\frac{d}{dt}i_r+j(\omega_{slip})(\sigma L_r i_r+\frac{L_m}{L_s}\psi_s) \tag{7}$$

Equation (7) in (d-q) reference frame components yields:

$$\begin{cases} \frac{d}{dt}\begin{bmatrix} I_{rd} \\ I_{rq} \end{bmatrix} = \begin{bmatrix} -\frac{R_r}{\sigma L_r} & \omega_{slip} \\ -\omega_{slip} & -\frac{R_r}{\sigma L_r} \end{bmatrix}\begin{bmatrix} I_{rd} \\ I_{rq} \end{bmatrix} \\ +\frac{L_m \omega_{slip}}{\sigma L_r L_s}\begin{bmatrix} \psi_{sq} \\ -\psi_{sq} \end{bmatrix} + \frac{1}{\sigma L_r}\begin{bmatrix} V_{rd} \\ V_{rq} \end{bmatrix} \end{cases} \quad (8)$$

The stator's output active power (p_s) and reactive power (q_s) can be calculated as;

$$\begin{cases} p_s + jq_s = -\frac{3}{2} V_{sdq}^{+} \times \hat{I}_{sdq}^{+} \approx -\frac{3}{2} j\omega_s \psi_s \times (\hat{\psi}_s - L_m I_r) \\ = -\frac{3}{2}\omega_s (j\psi_s) \times \frac{1}{L_s}[(\psi_s - L_m I_{rd}) + jL_m I_{rq}] \\ = \frac{3}{2}\frac{\omega_s}{L_s}[\psi_s L_m I_{rq} - j\psi_s(\psi_s - L_m I_{rd})] \end{cases} \quad (9)$$

Thus, the stator active and reactive powers are given by

$$p_s = \frac{3}{2}\frac{\omega_s}{L_s}\psi_s L_m I_{rq} \;,\; q_s = -\frac{3}{2}\frac{\omega_s}{L_s}\psi_s(\psi_s - L_m I_{rd}) \quad (10)$$

2.2. Unbalanced Grid Conditions:

Under unbalanced conditions, variable F in (α-β) reference frame can be described as follows:

$$\begin{cases} F_{\alpha\beta}(t) = F_{\alpha\beta+}(t) + F_{\alpha\beta-}(t) = \left|F_{\alpha\beta+}\right| e^{j(\omega_s t + \phi_+)} \\ + \left|F_{\alpha\beta-}\right| e^{-j(\omega_s t + \phi_-)} \end{cases} \quad (11)$$

Where ϕ_+ and ϕ_- are phase shifts in positive and negative sequences [1].

As shown in "Fig. 2", the conversions between the reference frame positive sequence (dq^+) and negative (dq^-) are given as follows:

$$F_{dq}^{+} = F_{dq}^{-} e^{-2j\omega_s t}, \; F_{dq}^{-} = F_{dq}^{+} e^{2j\omega_s t} \quad (12)$$

According to (11), variable F is the sum of the positive and negative sequences. Therefore, in the reference frame (dq^+), variable F in (12) can be written as follows:

$$F_{dq}^{+} = F_{dq+}^{+} + F_{dq-}^{+} = F_{dq+}^{+} + F_{qd-}^{-} e^{-2j\omega_s t} \quad (13)$$

According to (13), the positive component is a constant value and the negative component oscillates with frequency ($2\omega_s$) [5]-[7]. Equation (13) can be expressed as a constant value and an oscillatory value:

$$\begin{cases} F_d^{+} = F_{d+}^{+} + F_{d-}^{-}\cos 2\omega_s t + F_{q-}^{-}\sin 2\omega_s t \\ F_q^{+} = F_{q+}^{+} + F_{q-}^{-}\cos 2\omega_s t - F_{d-}^{-}\sin 2\omega_s t \end{cases} \quad (14)$$

The stator's output active power and reactive power in the positive sequence reference frame is :

$$p_s + jq_s = -\frac{3}{2} V_{sdq}^{+} \times \hat{I}_{sdq}^{+} = -\frac{3}{2}\left(V_{sq}^{+} - jV_{sd}^{+}\right)\left(I_{sq}^{+} + jI_{sd}^{+}\right) \quad (15)$$

Where,

$$\begin{cases} V_{sd}^{+} = -\omega_s \Psi_{sq}^{+} + \frac{d}{dt}\Psi_{sd}^{+} = \\ -\omega_s(\Psi_{sq+}^{+} + \Psi_{sq-}^{-}\cos 2\omega_s t - \Psi_{sd-}^{-}\sin 2\omega_s t) \\ + \frac{d}{dt}(\Psi_{sd+}^{+} + \Psi_{sd-}^{-}\cos 2\omega_s t + \Psi_{sq-}^{-}\sin 2\omega_s t) \\ = -\omega_s \Psi_{sq+}^{+} + \omega_s \Psi_{sq-}^{-}\cos 2\omega_s t - \omega_s \Psi_{sd-}^{-}\sin 2\omega_s t \end{cases} \quad (16)$$

$$\begin{cases} I_{sd}^{+} = \frac{1}{L_s}[\Psi_{sd}^{+} - L_m I_{rd}^{+}] = \\ \frac{1}{L_s}[(\Psi_{sd+}^{+} + \Psi_{sd-}^{-}\cos 2\omega_s t + \Psi_{sq-}^{-}\sin 2\omega_s t) \\ -L_m(I_{rd+}^{+} + I_{rd-}^{-}\cos 2\omega_s t + I_{rq-}^{-}\sin 2\omega_s t)] \end{cases} \quad (17)$$

$$\begin{cases} V_{sq}^{+} = \omega_s \Psi_{sd}^{+} + \frac{d}{dt}\Psi_{sq}^{+} = \\ \omega_s(\Psi_{sd+}^{+} + \Psi_{sd-}^{-}\cos 2\omega_s t + \Psi_{sq-}^{-}\sin 2\omega_s t) \\ + \frac{d}{dt}(\Psi_{sq+}^{+} + \Psi_{sq-}^{-}\cos 2\omega_s t - \Psi_{sd-}^{-}\sin 2\omega_s t) \\ = \omega_s \Psi_{sq+}^{+} - \omega_s \Psi_{sd-}^{-}\cos 2\omega_s t - \omega_s \Psi_{sq-}^{-}\sin 2\omega_s t \end{cases} \quad (18)$$

$$\begin{cases} I_{sq}^{+} = \frac{1}{L_s}[\Psi_{sq}^{+} - L_m I_{rq}^{+}] = \\ \frac{1}{L_s}[(\Psi_{sq+}^{+} + \Psi_{sq-}^{-}\cos 2\omega_s t - \Psi_{sd-}^{-}\sin 2\omega_s t) \\ -L_m(I_{rq+}^{+} + I_{rq-}^{-}\cos 2\omega_s t - I_{rd-}^{-}\sin 2\omega_s t)] \end{cases} \quad (19)$$

In DFIG, we assume that the stator resistance is negligible. Therefore, in reference (dq^+) :

$$\begin{cases} V_{sdq}^{+}=\dfrac{d}{dt}\Psi_{sdq}^{+}+j\omega_s\Psi_{sdq}^{+} \\ =\dfrac{d}{dt}(\Psi_{sdq+}^{+}+\Psi_{sdq-}^{-}e^{-2j\omega_s t}) \\ +j\omega_s(\Psi_{sdq+}^{+}+\Psi_{sdq-}^{-}e^{-2j\omega_s t}) \\ =j\omega_s\Psi_{sdq+}^{+}-j\omega_s\Psi_{sdq-}^{-}e^{-2j\omega_s t}=V_{sdq+}^{+}+V_{sdq-}^{-}e^{-2j\omega_s t} \end{cases} \quad (20)$$

Therefore:

$$\begin{cases} V_{sdq+}^{+}=j\omega_s\Psi_{sdq+}^{+}\Rightarrow\left(V_{sq+}^{+}-jV_{sd+}^{+}\right)=j\omega_s\left(\Psi_{sq+}^{+}-j\Psi_{sd+}^{+}\right) \\ V_{sdq-}^{-}=-j\omega_s\Psi_{sdq-}^{-}\Rightarrow\left(V_{sq-}^{-}-jV_{sd-}^{-}\right)=-j\omega_s\left(\Psi_{sq-}^{-}-j\Psi_{sd-}^{-}\right) \end{cases} \quad (21)$$

And:

$$\begin{cases} \Psi_{sd+}^{+}=\dfrac{1}{\omega_s}V_{sq+}^{+},\ \Psi_{sq+}^{+}=\dfrac{-1}{\omega_s}V_{sd+}^{+} \\ \Psi_{sd-}^{-}=\dfrac{-1}{\omega_s}V_{sq-}^{-},\ \Psi_{sq-}^{-}=\dfrac{1}{\omega_s}V_{sd-}^{-} \end{cases} \quad (22)$$

According to (14), although unbalanced, the stator voltage can still be regarded as constant (F_{d+}^{+} , F_{q+}^{+}). Consequently:

$$\begin{cases} \dfrac{d}{dt}\left(\Psi_{sd+}^{+}\right)=0,\ \dfrac{d}{dt}\left(\Psi_{sd-}^{-}\right)=0 \\ \dfrac{d}{dt}\left(\Psi_{sq+}^{+}\right)=0,\ \dfrac{d}{dt}\left(\Psi_{sq-}^{-}\right)=0 \end{cases} \quad (23)$$

By replacing relations (22) into (16, 17, 18 and 19) and considering Relation (23), active and reactive power can be expressed as:

$$\begin{cases} p_s=P_{s\text{-}av}+P_{s\text{-}sin2}\sin(2\omega_s t)+P_{s\text{-}cos2}\cos(2\omega_s t) \\ q_s=Q_{s\text{-}av}+Q_{s\text{-}sin2}\sin(2\omega_s t)+Q_{s\text{-}cos2}\cos(2\omega_s t) \end{cases} \quad (24)$$

Considering that in VOC control $V_{sq+}^{+}=0$, the active and reactive matrix form can be described as [4]:

$$\begin{cases} \begin{bmatrix} P_{s\text{-}av} \\ P_{s\text{-}sin2} \\ P_{s\text{-}cos2} \end{bmatrix}=\dfrac{3}{2\omega_s L_s}\begin{bmatrix} 0 \\ -2V_{sd-}^{-}V_{sd+}^{+} \\ 2V_{sq-}^{-}V_{sd+}^{+} \end{bmatrix} \\ +\dfrac{3L_m}{2L_s}\begin{bmatrix} V_{sd+}^{+} & 0 & V_{sd-}^{-} & V_{sq-}^{-} \\ V_{sq-}^{-} & -V_{sd-}^{-} & 0 & V_{sd+}^{+} \\ V_{sd-}^{-} & V_{sq-}^{-} & V_{sd+}^{+} & 0 \end{bmatrix}\begin{bmatrix} I_{rd+}^{+} \\ I_{rq+}^{+} \\ I_{rd-}^{-} \\ I_{rq-}^{-} \end{bmatrix} \end{cases} \quad (25)$$

$$\begin{bmatrix} Q_{s\text{-}av} \\ Q_{s\text{-}sin2} \\ Q_{s\text{-}cos2} \end{bmatrix}=\dfrac{3}{2\omega_s L_s}\begin{bmatrix} -(V_{sd+}^{+})^2+(V_{sd-}^{-})^2+(V_{sq-}^{-})^2 \\ 0 \\ 0 \end{bmatrix}\begin{bmatrix} I_{rd+}^{+} \\ I_{rq+}^{+} \\ I_{rd-}^{-} \\ I_{rq-}^{-} \end{bmatrix} \quad (26)$$

The electromagnetic torque (T_e) of a DFIG can be described as:

$$\begin{cases} T_e=\dfrac{3}{2}P\mathrm{Im}[\psi_s(t)i_s^{*}(t)]= \\ \dfrac{3}{2}P\mathrm{Im}\left[\psi_s(t)\left\{\psi_s^{*}(t)-L_m i_r^{*}(t)\right\}\right]= \\ -\dfrac{3PL_m}{2L_s}\mathrm{Im}[\psi_s(t)i_r^{*}(t)] \end{cases} \quad (27)$$

(P is pole pair), where the matrix form of electromagnetic torque is:

$$\begin{cases} \begin{bmatrix} T_{e\text{-}av} \\ T_{e\text{-}sin2} \\ T_{e\text{-}cos2} \end{bmatrix}=\dfrac{3L_m}{2L_s\omega_s}\begin{bmatrix} V_{sd+}^{+} & 0 & -V_{sd-}^{-} & -V_{sq-}^{-} \\ -V_{sq-}^{-} & V_{sd-}^{-} & 0 & V_{sd+}^{+} \\ -V_{sd-}^{-} & -V_{sq-}^{-} & V_{sd+}^{+} & 0 \end{bmatrix} \\ \begin{bmatrix} I_{rd+}^{+} \\ I_{rq+}^{+} \\ I_{rd-}^{-} \\ I_{rq-}^{-} \end{bmatrix} \end{cases} \quad (28)$$

3. CONTROL OF RSC

3.1. Balanced Conditions

Equation (10) indicates active power controlled by regulating (I_{rq}) and reactive power can be controlled by regulating (I_{rd}). As a result, the active and reactive power can be controlled independently using rotor current (I_{rq}) and (I_{rd}), respectively. According to (8), the required rotor control voltages in the (d-q) reference frame are given by [8]-[9]:

$$\begin{cases} \begin{bmatrix} V_{rd} \\ V_{rq} \end{bmatrix}=\sigma L_r\dfrac{d}{dt}\begin{bmatrix} I_{rd} \\ I_{rq} \end{bmatrix} \\ -\sigma L_r\begin{bmatrix} -\dfrac{R_r}{\sigma L_r} & \omega slip \\ -\omega slip & -\dfrac{R_r}{\sigma L_r} \end{bmatrix}\begin{bmatrix} I_{rd} \\ I_{rq} \end{bmatrix} \\ -\dfrac{L_m\omega slip}{L_s}\begin{bmatrix} \psi sq \\ -\psi sq \end{bmatrix} \end{cases} \quad (29)$$

Where:

$$\begin{cases} \dfrac{d}{dt}\begin{bmatrix} I_{rd} \\ I_{rq} \end{bmatrix}= \\ (I_{rdq}(ref)-I_{rdq})(k_{pd}+k_{id}\int(I_{rdq}(ref)-I_{rdq}) \end{cases} \quad (30)$$

Where, k_{pd} and k_{id} are the proportional and integral gains of the current controllers.

3.2. Unbalanced Conditions

Under unbalance grid conditions, the negative sequence component of stator voltage leads to the oscillation of power (active-reactive) and electromagnetic torque with frequency ($2\omega_s$). Power fluctuations lead to increased temperature in the stator winding, and torque fluctuations lead to mechanical tension on the rotor. In order to make the steady-state error value zero and improve the accuracy of controlling, Proportional-Integral (PI) controller is used. As the simultaneous elimination of power and torque oscillations are not possible, the controller is set to Target 1 (Eliminating fluctuation of stator active power) and Target 2 (Eliminating fluctuation of electromagnetic torque).

Target 1: According to (25), the required negative sequence rotor current leads to ($P_{s\text{-}sin2}=0, P_{s\text{-}cos2}=0$)given as

$$\begin{cases} P_{s\text{-}sin2}=0 \Rightarrow \\ I^{-}_{rq-}(ref)=\dfrac{1}{V^{+}_{sd+}}\left(V^{-}_{sd-}I^{+}_{rq+}-V^{-}_{sq-}I^{+}_{rd+}\right)+\dfrac{2V^{-}_{sd-}}{\omega_s L_m} \end{cases} \quad (31)$$

$$\begin{cases} P_{s\text{-}cos2}=0 \Rightarrow \\ I^{-}_{rd-}(ref)=\dfrac{-1}{V^{+}_{sd+}}\left(V^{-}_{sd-}I^{+}_{rd+}+V^{-}_{sq-}I^{+}_{rq+}\right)-\dfrac{2V^{-}_{sq-}}{\omega_s L_m} \end{cases} \quad (32)$$

Accordingly, power (active-reactive) and the electromagnetic torque are given by:

$$P_{s\_av}=\frac{3L_m}{2L_s}\frac{\left((V^{+}_{sd+})2-(V^{-}_{sd-})2-(V^{-}_{sq-})2\right)}{V^{+}_{sd+}}I^{+}_{rd+} \quad (33)$$

$$\begin{cases} Q_{s\text{-}av}=-\dfrac{3}{2L_s}\dfrac{\left((V^{-}_{sd-})2+(V^{-}_{sq-})2+(V^{+}_{sd+})2\right)}{V^{+}_{sd+}} \\ \left(\dfrac{V^{+}_{sd+}}{\omega_s}+L_m I^{+}_{rq+}\right) \end{cases} \quad (34)$$

$$T_{e\text{-}av}=\frac{3PL_m}{2\omega_s L_s}\frac{\left((V^{+}_{sd+})2+(V^{-}_{sd-})2+(V^{-}_{sq-})2\right)}{V^{+}_{sd+}}I^{+}_{rd+} \quad (35)$$

Target2: In this case, mechanical tension on the rotor decreases. According to (28), the required negative sequence rotor current leads to ($T_{e\text{-}sin2}=0, T_{e\text{-}cos2}=0$) given as:

$$T_{e\text{-}sin2}=0 \Rightarrow I^{-}_{rq-}(ref)=\frac{1}{V^{+}_{sd+}}\left(V^{-}_{sq-}I^{+}_{rd+}-V^{-}_{sd-}I^{+}_{rq+}\right) \quad (36)$$

$$T_{e\text{-}cos2}=0 \Rightarrow I^{-}_{rd-}(ref)=\frac{1}{V^{+}_{sd+}}\left(V^{-}_{sd-}I^{+}_{rd+}+V^{-}_{sq-}I^{+}_{rq+}\right) \quad (37)$$

Therefore, power (active-reactive) and the electromagnetic torque are given by:

$$P_{e\text{-}av}=\frac{3L_m}{2L_s}\frac{\left((V^{+}_{sd+})2+(V^{-}_{sd-})2+(V^{-}_{sq-})2\right)}{V^{+}_{sd+}}I^{+}_{rd+} \quad (38)$$

$$\begin{cases} Q_{s\text{-}av}=-\dfrac{3}{2L_s}\dfrac{\left((V^{-}_{sq-})2-(V^{-}_{sq-})2-(V^{+}_{sd+})2\right)}{V^{+}_{sd+}} \\ \left(\dfrac{V^{+}_{sd+}}{\omega_s}+L_m I^{+}_{rq+}\right) \end{cases} \quad (39)$$

$$T_{e\text{-}av}=\frac{3PL_m}{2\omega_s L_s}\frac{\left((V^{+}_{sd+})2-(V^{-}_{sd-})2-(V^{-}_{sq-})2\right)}{V^{+}_{sd+}}I^{+}_{rd+} \quad (40)$$

Equations (33, 34, 35) and (38, 39, 40) express active power and electromagnetic torque controlled by regulating (I^{+}_{rd+}) and reactive power can be controlled by regulating (I^{+}_{rq+}). In the meanwhile, controlling (I^{-}_{rd-}) and (I^{-}_{rq-}) can eliminate the oscillations of either stator active power based on (31, 32) or electromagnetic torque based on (36, 37). As a result, the average power and electromagnetic torque can be controlled independently using the rotor current positive sequence component (I^{+}_{rd+}, I^{+}_{rq+}) and the oscillation can be eliminated by using the rotor current negative sequence component (I^{-}_{rd-}, I^{-}_{rq-}). “Fig. 3” shows the block diagram phase-locked loop (PLL). The stator's voltage frequency (ω_s), the phase angle of the stator voltage (θ_s), negative, and positive sequence components of stator voltage and the negative and positive sequence components of the rotor current can be measured by PLL. Under unbalance grid conditions, to reduce the effects of the negative sequence component, the band stop filter (B.S.F) with twice the grid frequency is used. “Fig.4” shows the block diagram of a Voltage Orientation Control (VOC) for RSC control under unbalanced grid. The purpose of control RSC is to eliminate power fluctuations (Target 1) and torque fluctuations

(Target 2). To achieve Target 1, control components' positive and negative sequences can be calculated by (33, 34, 35) and (31, 32), respectively. To achieve Target 2, components' positive and negative sequences can be calculated by (38, 39, 40) and (36, 37), respectively.

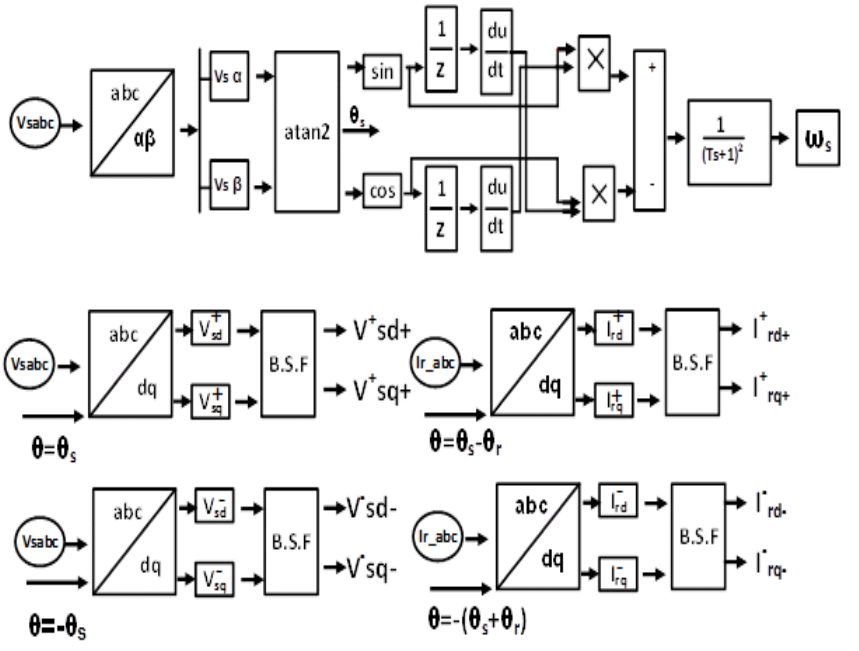

Fig. 3. Block diagram of the phase-locked loop (PLL)

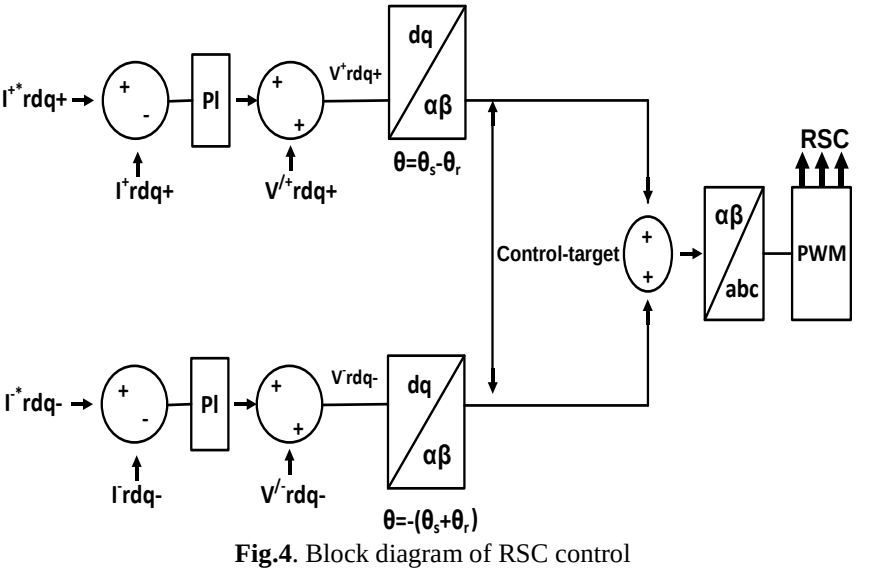

Fig.4. Block diagram of RSC control

Where:

$$V_{rd} = \frac{d}{dt}\Psi_{rd} - (\omega_{slip})\Psi_{rq} + R_r i_{rd} \quad (41)$$

$$Vrq = \frac{d}{dt}\Psi rq - (\omega_{slip})\Psi rd + R_r i_{rq} \quad (42)$$

$$\begin{cases} \Psi_{rd} = L_r i_{rd} + L_m i_{sd} = \\ L_r i_{rd} + \frac{L_m}{L_s}\left(\Psi_{sd} - L_m i_{rd}\right) = \\ \sigma L_r i_{rd} + \frac{L_m}{L_s}\Psi_{sd} \end{cases} \quad (43)$$

$$\begin{cases} \Psi_{rq} = L_r i_{rq} + L_m i_{sq} = \\ L_r i_{rq} + \frac{L_m}{L_s}\left(\Psi_{sq} - L_m i_{rd}\right) = \\ \sigma L_r i_{rq} + \frac{L_m}{L_s}\Psi_{sq} \end{cases} \quad (44)$$

With substituting (41) and (42) into (43) and (44) control voltages are given by:

$$\begin{cases} V_{rd+}^{+}(ref) = \sigma L_r \frac{d}{dt} i_{rq+}^{+} + V'^{+}_{rd+}, \\ V'^{+}_{rd+} = -(\omega_{slip})\sigma L_r i_{rq+}^{+} + \frac{\omega_{slip} L_m}{\omega_s L_s} V_{sd+}^{+} \end{cases} \quad (45)$$

$$\begin{cases} V_{rq+}^{+}(ref) = \sigma L_r \frac{d}{dt} i_{rd+}^{+} + V'^{+}_{rq+}, \\ V'^{+}_{rq+} = (\omega_{slip})\sigma L_r i_{rd+}^{+} - \frac{\omega_{slip} L_m}{\omega_s L_s} V_{sq+}^{+} \end{cases} \quad (46)$$

$$\begin{cases} V_{rd-}^{-}(ref) = \sigma L_r \frac{d}{dt} i_{rq-}^{-} + V'^{-}_{rd-} \\ V'^{-}_{rd-} = -(\omega_{slip})\sigma L_r i_{rq-}^{-} - \frac{\omega_{slip} L_m}{\omega_s L_s} V_{sd-}^{-} \end{cases} \quad (47)$$

$$\begin{cases} V_{rq-}^{-}(ref) = \sigma L_r \frac{d}{dt} i_{rq-}^{-} + V'^{+}_{rq+} \\ V'^{-}_{rq-} = (\omega_{slip})\sigma L_r i_{rd-}^{-} - \frac{\omega_{slip} L_m}{\omega_s L_s} V_{sq-}^{-} \end{cases} \quad (48)$$

$$\frac{d}{dt}(I_{rdq}) = (I_{rdq}(ref) - I_{rdq})(k_{pd} + \frac{k_{id}}{s}) \quad (49)$$

Where, k_{pd} and k_{id} are the proportional and integral gains of the current controllers.

4. CONTROL OF GSC

To regulate DC-Link voltage, an Extended State Observer (ESO), based on a Generalized Proportional-Integral (GPI) controller, is employed. "Fig. 5" shows the block diagram of the ESO controller. In this controlling method, the voltage of the DC-Link, is controlled without requiring to measure the current of GSC and because of GPI, the dynamic response is improved, voltage-settling time is reduced, and it is resistant to changes in voltage parameters. Power transfer relationship in GSC can be described as:

$$\begin{cases} \frac{d}{dt}(0.5CV_{DC}^2) = -\frac{V_{DC}^2}{R_{loos}} - P_r(t) + P_g(t) \Rightarrow \\ V_{DC}^2(S) = \frac{2R_{loos}s}{CR_{loos}s+2} P_g(s) - \frac{2R_{loos}s}{CR_{loos}s+2} P_r(s) \end{cases} \quad (50)$$

$R_{loos} = R_p$ is the loss of switching, V_{DC} is voltage DC-Link, C is the capacity, P_r is output active power of the rotor, and $P_g \cong P_g(ref)$, where $P_g(ref)$ and P_g are reference and output power of GSC respectively.

4.1. Designing of ESO

"Fig. 6" shows the block diagram of voltage control of the DC-Link voltage by GSC. This diagram consists of an internal loop for controlling converter current and an external loop for controlling and regulating the DC-Link voltage [21]-[22]. In order to prevent dynamic interference between internal and external loops, the bandwidth of the internal loop is considered much larger than that of the external loop. Equation (50) can be rewritten as:

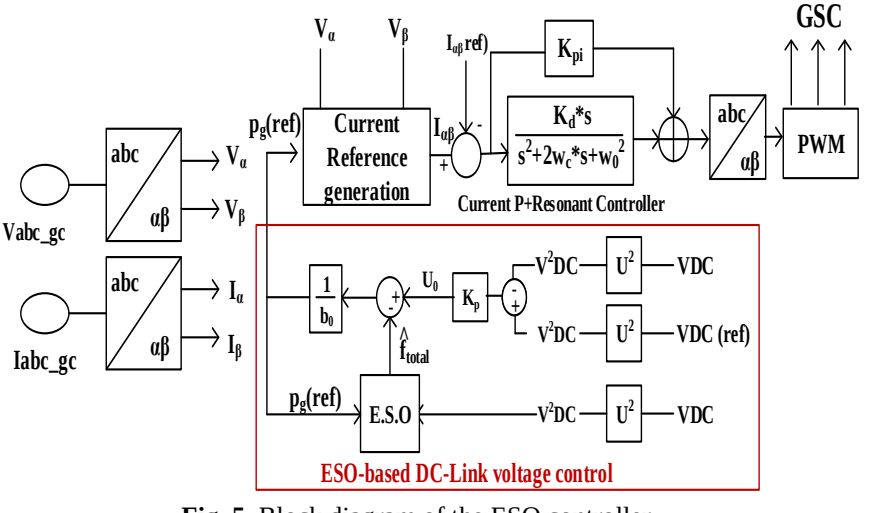

Fig. 5. Block diagram of the ESO controller.

$$\begin{cases} \frac{d}{dt}(V_{DC}^2)= \frac{2}{C}P_g(t)-\frac{2}{C}(\frac{V_{DC}^2}{R_{loos}}+P_r(t))= \\ \frac{2}{C}P_g(t)+f_{total} \end{cases} \quad (51)$$

Where, $f_{total} = -\frac{2}{C}(\frac{V_{DC}^2}{R_{loos}}+P_r(t))$ is a total disturbance that consists of the external disturbance $-\frac{2}{C}(P_r(t))$ and internally dynamic variation $-\frac{2}{C}(\frac{V_{DC}^2}{R_{loos}})$. In (51), V_{DC}^2 is considered as a state variable and expressed as $x_1 = V_{DC}^2$, f_{total} is considered as based on augmented input estimation (AIE) of state variable x_2 and expressed [21]-[22] as: $x_2 = f_{total} = -\frac{2}{C}(\frac{V_{DC}^2}{R_{loos}}+P_r(t))$ and $P_g(t)$ is the system input and indicated as: $u=P_g(t), b_0=\frac{2}{C}$ is the coefficient of input. Moreover, the derivative time of x_2 is signified h, and the expression is shown as: $\frac{dx_2}{dt}=h$ .Therefore, from the aforementioned analysis, the state-space model is derived as:

$$\begin{bmatrix} \dot{x}_1 \\ \dot{x}_2 \end{bmatrix} = \begin{bmatrix} 0 & 1 \\ 0 & 0 \end{bmatrix}\begin{bmatrix} x_1 \\ x_2 \end{bmatrix} + \begin{bmatrix} b_0 \\ 0 \end{bmatrix}u + \begin{bmatrix} 0 \\ 1 \end{bmatrix}h \quad (52)$$

Based on (57), the ESO is constructed as:

$$\begin{bmatrix} \dot{z}_1 \\ \dot{z}_2 \end{bmatrix} = \begin{bmatrix} 0 & 1 \\ 0 & 0 \end{bmatrix}\begin{bmatrix} z_1 \\ z_2 \end{bmatrix} + \begin{bmatrix} b_0 \\ 0 \end{bmatrix}u + \begin{bmatrix} \beta_1 \\ \beta_2 \end{bmatrix}\begin{bmatrix} x_1-z_1 \end{bmatrix} \quad (53)$$

Where, z_1, z_2 are the estimated values of x_1, x_2 and $\begin{bmatrix} \beta_1 \\ \beta_2 \end{bmatrix}$ is the gain vector of ESO. The state error equation (e_1 and e_2) can be subtracted (53) from (52), as follows:

$$\begin{bmatrix} \dot{e}_1 \\ \dot{e}_2 \end{bmatrix} = \begin{bmatrix} -\beta_1 & 1 \\ -\beta_2 & 0 \end{bmatrix}\begin{bmatrix} e_1 \\ e_2 \end{bmatrix} ++ \begin{bmatrix} 0 \\ 1 \end{bmatrix}h, \begin{bmatrix} -\beta_1 & 1 \\ -\beta_2 & 0 \end{bmatrix} = H_e \quad (54)$$

From (54), it is known that the matrix (H_e) will be Routh-Hurwitz stable if all the roots of the characteristic polynomial of H_e, i.e.:

$$\lambda(s)= s^2+\beta_1 s+\beta_2 \quad (55)$$

Are in the left half-plane. Suppose all poles of ESO are designed to stay on bandwidth ($-\omega_0$), which is indicated below [20]:

$$\lambda(s)= s^2+\beta_1 s+\beta_2 = (s+\omega_0)^2 \rightarrow \beta_1=2\omega_0, \beta_2=\omega_0^2 \quad (56)$$

From (56), it is shown that the design of ESO is simplified to tune the (ω_0) of the ESO, which greatly simplifies the design process. Choosing (ω_0) is an essential factor that affects the system's function. Observer's bandwidth is usually chosen 5 to 15 times of the bandwidth of the controller of the DC-Link voltage. Therefore, the dynamics of the estimated state has fast tracking performance. Since high bandwidth reduces safety versus system noise, the bandwidth of ESO cannot be very high. In order to achieve a fast dynamic response, the bandwidth of the current loop is chosen 300 rad/s, and the voltage controller of the DC-Link is chosen 20 rad/s. As a result, all three loops are separated, and ESO has a high dynamic response for estimating the real state.

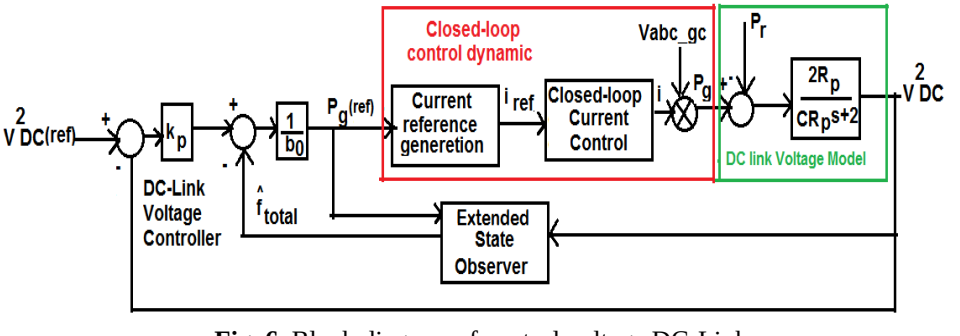

Fig. 6. Block diagram of control voltage DC-Link.

By substituting $\beta_1=2\omega_0$ and $\beta_2=\omega_0^2$ in (54), the ESO is described as:

$$\begin{bmatrix} \dot{z}_1 \\ \dot{z}_2 \end{bmatrix} = \begin{bmatrix} -2\omega_0 & 1 \\ -\omega_0^2 & 0 \end{bmatrix} \begin{bmatrix} z_1 \\ z_2 \end{bmatrix} + \begin{bmatrix} b_0 & 2\omega_0 \\ 0 & \omega_0^2 \end{bmatrix} \begin{bmatrix} u \\ x_1 \end{bmatrix} \quad (57)$$

Equation (57) is corresponded in the Laplace domain to "Fig. 7":

$$G_{f\text{-}u(s)} = \frac{\hat{f}_{total}(s)}{u(s)} = \begin{bmatrix} 0 & 1 \end{bmatrix} [SI\text{-}A_z]^{-1} \begin{bmatrix} b_0 \\ 0 \end{bmatrix} = -\frac{b_0\omega_0^2}{(s+\omega_0)^2} \quad (58)$$

$$G_{f\text{-}V_{DC}^2} = \frac{\hat{f}_{total}(s)}{V_{DC}^2} = \begin{bmatrix} 0 & 1 \end{bmatrix} [SI\text{-}A_z]^{-1} \begin{bmatrix} 2\omega_0 \\ \omega_0^2 \end{bmatrix} = \frac{s\omega_0^2}{(s+\omega_0)^2} \quad (59)$$

By combining (58) and (59), the transfer function of ESO would be as follows:

$$\hat{f}_{total}(s) = \frac{b_0\omega_0^2}{(s+\omega_0)^2} u(s) + \frac{s\omega_0^2}{(s+\omega_0)^2} V_{DC}^2 \quad (60)$$

5. PROPOSED FCL MODEL DESCRIPTION

In this paper, to enhance the transient performance of DFIG during a fault, two strategies are recommended, Fault Current Limiter (S-FCL) and Storage Fault Current Limiter (MES-FCL**)**.

5.1. Structure and Principle of the S-FCL

An arrangement to reduce the fault current by placing S-FCL between rotor windings and RSC is shown in "Fig. 8". At normal operating condition both the thyristors are turn off and inductor (L) with capacitor (C) are placed in series, in this condition the values of L, C are designed to be in resonance with the frequency network. However, at fault condition, both the thyristors are turn on and current flows through the inductor path and limit the increasing rate of fault current. This value of inductor impedance limits the fault current and also improves the terminal voltage of DFIG.

5.2. Structure and Principle of the MES-FCL

"Fig. 9" shows the block diagram of MES-FCL. Under fault conditions, switches S1 and S2 turn on, diode (D) is revers biased, current input signals to the RSC is blocked and the input mechanical energy of the turbine is stored in inductor (L) as electromagnetic energy. After fault removal, switches S1 and S2 turn off, the diode (D) is directly biased and the energy stored in the inductor is transmitted to the DC-link capacitor (C). As a result, the balance is created between electrical and mechanical quantities. Therefore, the rotor speed deviation, electromagnetic torque fluctuations and requires reactive power are reduced and LVRT capability of DFIG is improved. One of the most important advantages of this MES-FCL is that, after fault removal, the electromagnetic energy stored in the inductor is transmitted to the DC-link capacitor. Therefore, the capacitor will not be charged by the GSC converter and GSC is used for fast voltage restoration of DFIG.

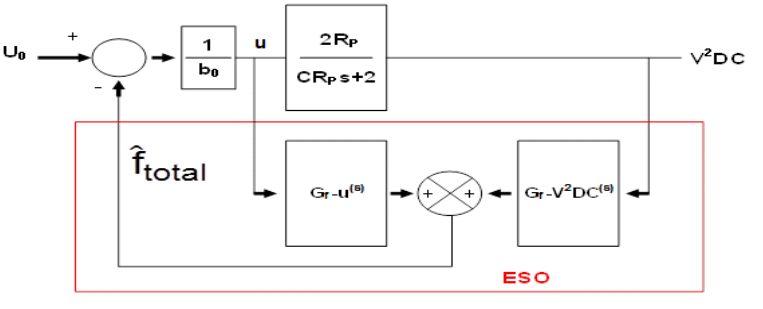

Fig. 7. Block diagram equivalent transfer function of ESO.

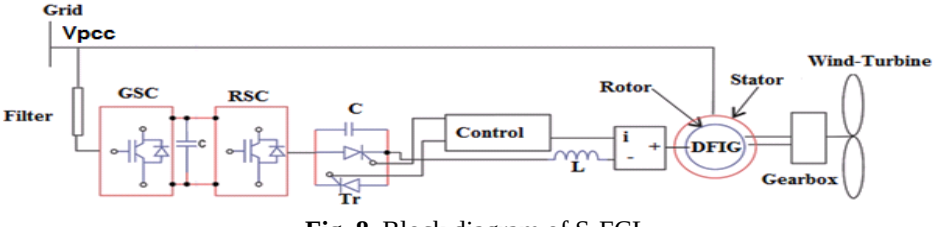

Fig. 8. Block diagram of S-FCL.

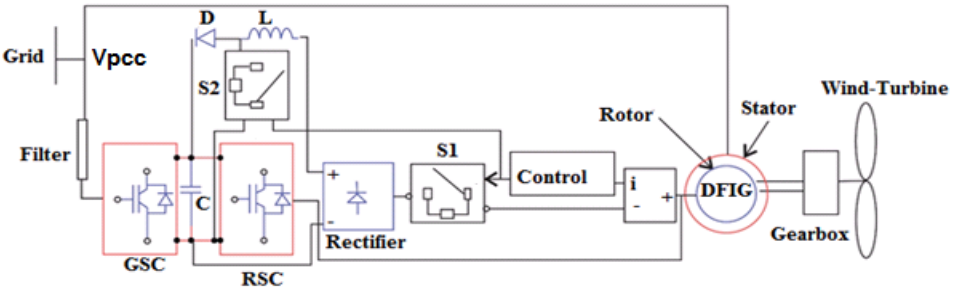

Fig. 9. Block diagram of MES-FCL.

5.3. MES-FCL Design Calculation

To ensure the better performance and least disturbance during fault condition, the energy stored in the inductor must be at least to the energy lost in the crowbar resistance.

$$E_{cw}=I_{rdc}^2*R_{cw}*t_f \ , E_L=\frac{1}{2}LI_{rdc}^2 \quad (61)$$

$$E_L \le E_{cw} \Rightarrow L \le 2*R_{cw}*t_f \quad (62)$$

R_{CW} is crowbar resistor, E_{CW} is energy lost in the crowbar resistance, E_L is energy stored in the inductor (L), t_f is fault duration and I_{rdc} is rotor current rectifier. For simulation analysis, the value of $R_{CW}=10*R_r$ or $R_{CW}=5*R_s$ where R_r and R_s are the resistor or rotor and stator of DFIG, respectively.

5.4. Control Technique

Without the faulty condition, sometimes the common coupling voltage decreases due to low demand and sometimes current is increased than its rated value. If only one term (voltage or current) has been considered for control strategy, then without fault condition FCL may work which is undesirable. Again during fault condition, both terminal voltage and current are affected. For that reason, for controlling the FCL both the terms should be considered. Firstly the value of reference voltage (V_{ref}) and current (I_{ref}) is predetermined. The value of V_{ref} is set to be 90% of the nominal value of V_{pcc}. Fault may be considered under the value of V_{ref} and above the value of I_{ref}. Thus Common coupling voltage V_{pcc} is compared with V_{ref} and line current I_{line} is compared with I_{ref} as shown in "Fig. 10".

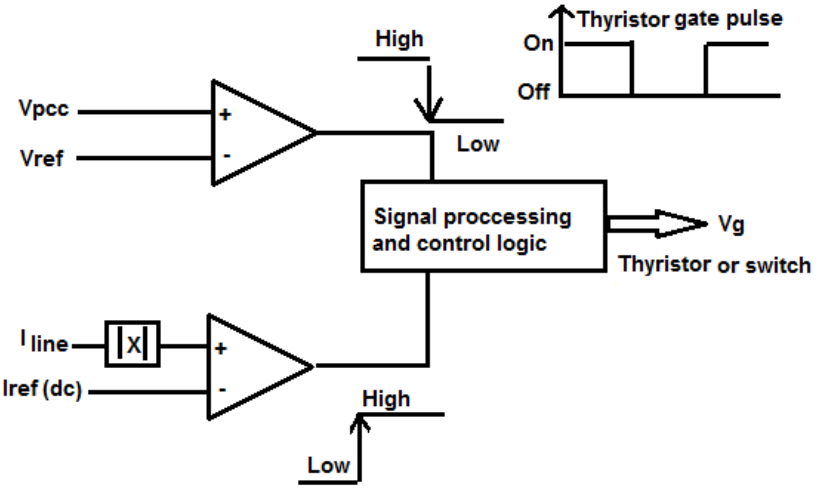

Fig. 10. FCL control.

6. SIMULATION RESULTS

Simulations of the proposed control strategy, for a DFIG-based generation system, were carried out using Matlab/Simulink. "Fig. 10", shows the schematic diagram of the implemented system. The DFIG was rated at (2 MW) and its parameters are given in Table I. The nominal converter DC- link voltage was set at (1200 V), the switching frequencies for both converters were (2 kHz), the rotor speed is (1.1pu) and wind speed is (16.2m/s). As shown in "Fig. 11", to absorb the switching harmonics generated by the two

converters to the stator side, a high-frequency AC filter is connected.

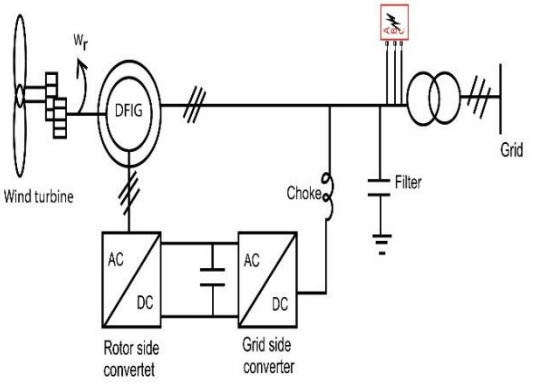

Fig. 11. Schematic diagram of the simulated system.

Table 1. DFIG parameters.

DFIG	Rated power	2MW
	voltage /Frequency	690V /5Hz
	R_S/R_r	0.0108pu /0.12pu
	L_m	3.362pu
	$L_{\sigma s}/L_{\sigma r}$	0.102pu /0.11pu
	Inertia constant	1.5s
Dc-link Capacitor	C_{dc}	0.0001F
Choke	L_g	0.25mH
Filter	$\mathbb{R}_f/C_f$	0.06Ω /1000 μF

The main objective of the RSC is to control active-reactive power and torque, in this paper, in order to achieve zero state error it was controlled using a Proportional-Integral (PI) controller. In the simulation, unbalanced grid conditions as a short circuit single line to ground fault in time duration at [3s-3.2s] was applied. Under unbalanced grid conditions for the conventional control scheme, it can be seen from "Fig. 12" voltage, current of stator and rotor current becomes unbalanced. "Fig. 13" shows the positive component of stator voltage (Vspd) and the negative sequence component of stator voltage (Vsnd, Vsnq) conventional control. Also, "Fig. 14" shows the positive component of rotor current (Irpd, Irpq) and negative sequence component of rotor current (Irnd, Irnq) conventional control. Under unbalance grid conditions, the negative sequence component of stator voltage and rotor current lead to the oscillation of power (active-reactive) and electromagnetic torque with frequency ($2\,\omega_s$ =100HZ). "Fig. 15" shows the power (active-reactive) and electromagnetic torque conventional control. Power fluctuations lead to increased temperature in the stator winding and torque fluctuations lead to mechanical tension on the rotor. To reduce the effects caused by the negative sequence component, the band stop filter is employed with twice the grid frequency. "Fig. 16" shows the positive and negative sequence components of stator voltage proposed control and "Fig. 17" shows the positive and negative sequence components of the rotor current after passing from the band stop filter. As the simultaneous elimination of power and torque oscillations by RSC is not possible, the controller of RSC is set to Target 1(Eliminating fluctuation of stator active power) during [3s-3.1s] and switched to Target 2 (Eliminating fluctuation of electromagnetic torque) during [3.1s-3.2s]. As can be seen in "Fig. 18", oscillations of the active power and torque have been reduced significantly during [3s-3.1s] and [3.1s-3.2s], respectively. The main objective of the Grid Side Converter (GSC) is to control the DC- link voltage, and it was controlled using an Extended State Observer (ESO) based on a Generalized Proportional-Integral (GPI) controller. To prove the results of the simulation, control of GSC with ESO controller is compared with the methods PI and proportional (P) controller. "Fig. 19" shows the DC- link voltage. As can be seen in the ESO proposed to control for GSC control, the maximum overshoot of DC-Link voltage in this controller is less than the maximum overshoot of DC-Link voltage when PI and P controller was employed. Also in ESO controller, due to using the GPI controller, settling time was reduced, and voltage changes in duration [3s-3.2s] were less than when the PI and P controller was employed. Therefore, the simulation results confirmed that the ESO controller for GSC control had a better behavior than in the other controller.

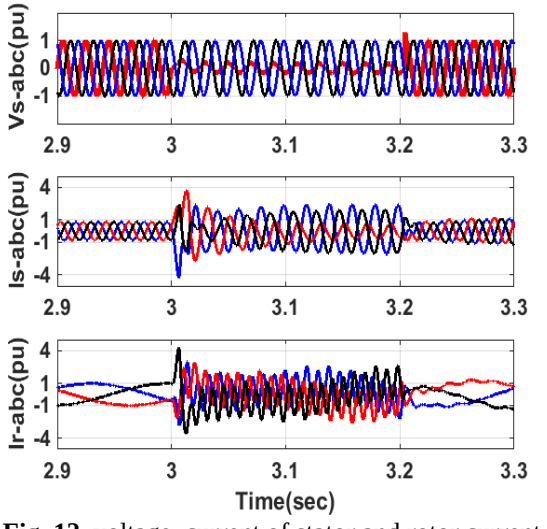

Fig. 12. voltage, current of stator and rotor current.

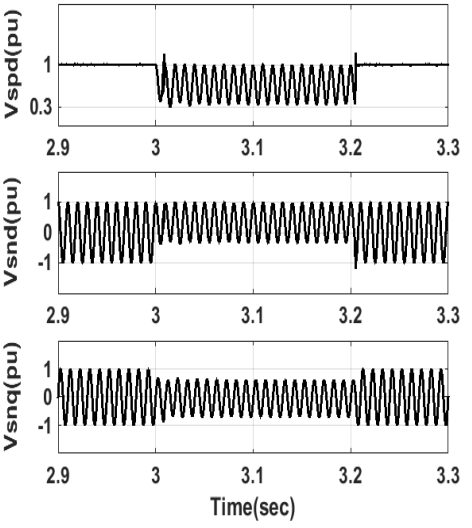

Fig. 13. Stator voltage sequence conventional control.

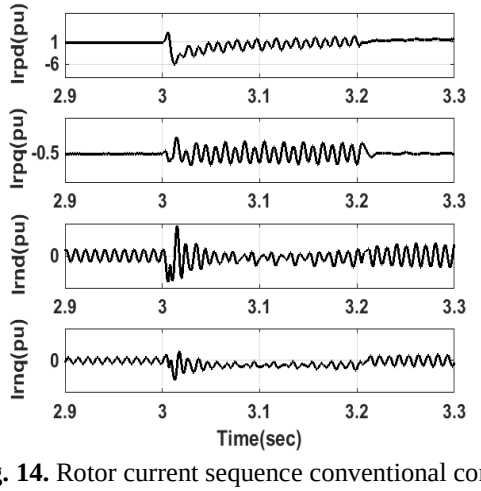

Fig. 14. Rotor current sequence conventional control.

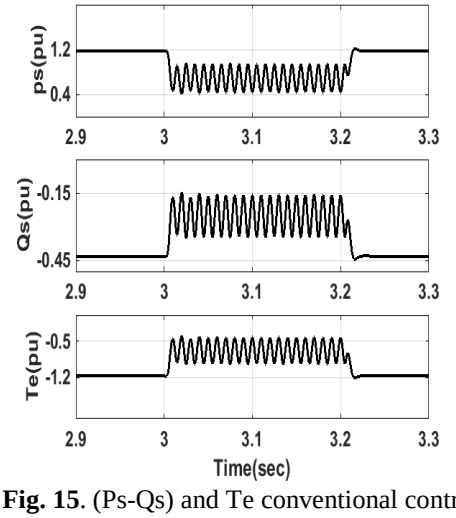

Fig. 15. (Ps-Qs) and Te conventional control.

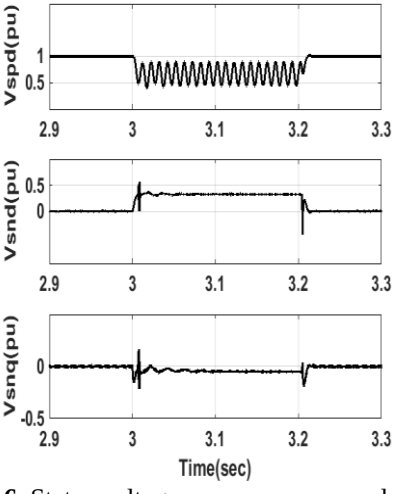

Fig. 16. Stator voltage sequence proposed control.

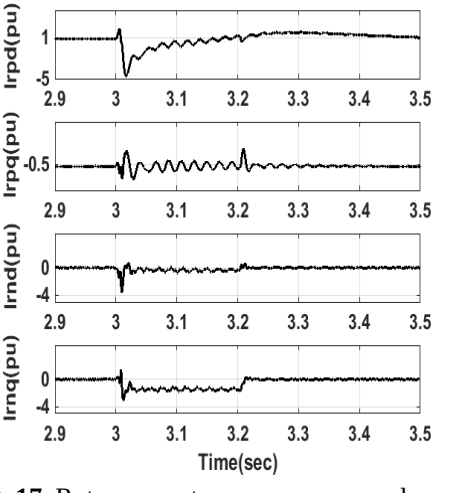

Fig. 17. Rotor current sequence proposed control.

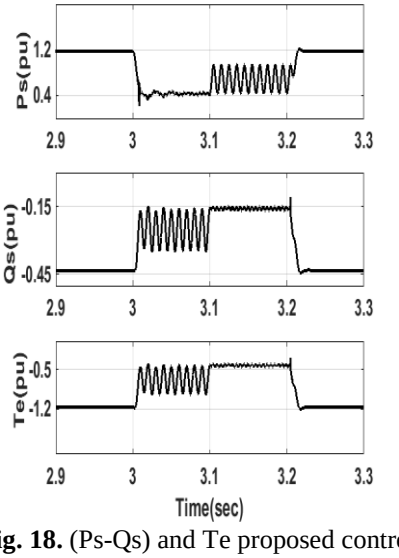

Fig. 18. (Ps-Qs) and Te proposed control.

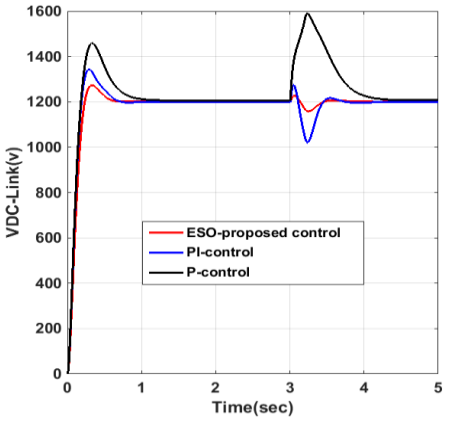

Fig. 19. Voltage DC-Link.

In this paper, to enhance Low Voltage Ride-Through (LVRT) Capability and transient performance of DFIG during a fault, two strategies are recommended, fault current limiter (S-FCL) and storage fault current limiter (MES-FCL**).** The performance of the proposed FCL is compared with that of the crowbar limiter (C-FCL) to determine the effectiveness of proposed FCL. For the purpose of transient analysis, A 2 MW DFIG based wind turbine is used and a three phase line-to-ground (3LG) fault is occurred at point F near the PCC as shown in "Fig.20", the 3LG fault of DFIG is considered as the most unfavorable condition. The 3LG fault at point F is occurred at t=3s for 200ms. "Fig. 21" shows the grid code requirement set by Federal Energy Regulatory commission.

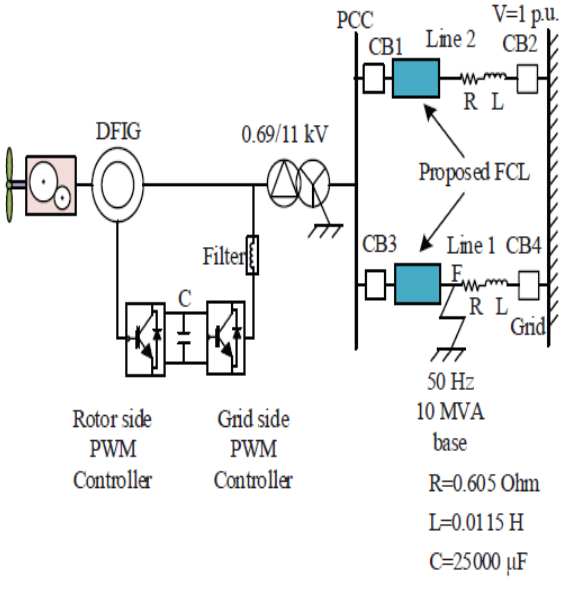

Fig. 20. Schematic diagram of DFIG with proposed FCL.

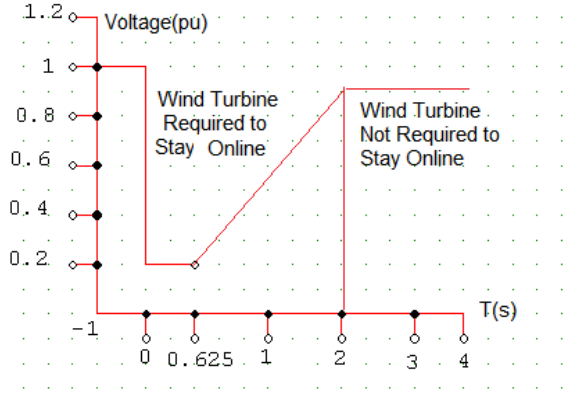

Fig. 21. LVRT standard set by FERC, U.S.

"Fig. 22" represents terminal voltage response of DFIG when a temporary 3LG fault is occurred. Without considering any controller terminal voltage decreases after the fault started and decreases lower and lower till the circuit breakers open. But using the MES-FCL, it maintains the voltage level to ± 1 p.u of nominal voltage. C-FCL does not maintain the voltage level as quickly as the proposed FCL. Thus proposed FCL can maintain grid code. "Fig. 23" shows the active power response of DFIG for 3LG fault. Without any controller, when the fault occurs output power decreases and becomes very close to zero. After opening the breaker, it causes huge imbalance of output power. Using the C-FCL and S-FCL output power goes very low at faulty condition and after opening the breaker it suddenly increased the output power which may have bad impact on the machine. But applying the MES-FCL, output power fluctuation is very low at fault and after opening the breaker. The proposed FCL provided faster stability than C-FCL and S-FCL. "Fig. 24" shows the faulted line current (C phase current) without any controller, with C-FCL and S-FCL with the MES-FCL. Without any controller faulted line current increased abruptly during 3LG fault. All S-FCL, C-FCL and MES FCL limit the fault current. But applying the MES-FCL fault current is better limited than S-FCL and C-FCL. "Fig. 25" shows the reactive power and "Fig. 26" shows the electromagnetic torque response of DFIG for 3LG fault. In MES-FCL, after fault removal, the energy stored in the inductor is transmitted to the DC-link capacitor (C). As a result, a balance is created between electrical and mechanical quantities. Therefore, electromagnetic torque fluctuations and required reactive power are reduced and LVRT capability of DFIG is improved than S-FCL and C-FCL. "Fig. 27" shows the voltage DC-Link. In MES-FCL, after fault removal, the electromagnetic energy stored in the inductor is transmitted to the DC-link capacitor, so the capacitor will not be charged by the GSC converter and GSC is used for fast voltage restoration of DFIG,

therefor under fault conditions increase of the voltage DC-Link is less than S-FCL and C-FCL.

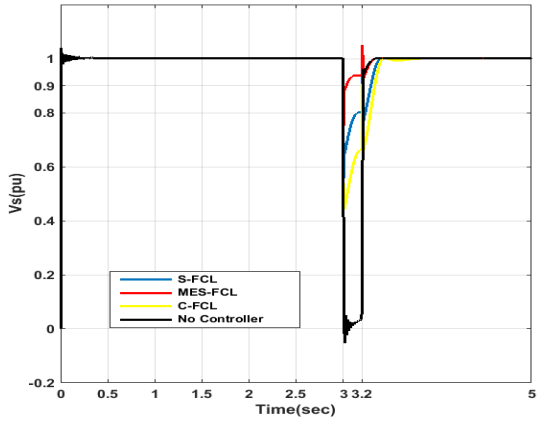

Fig. 22. Stator voltage.

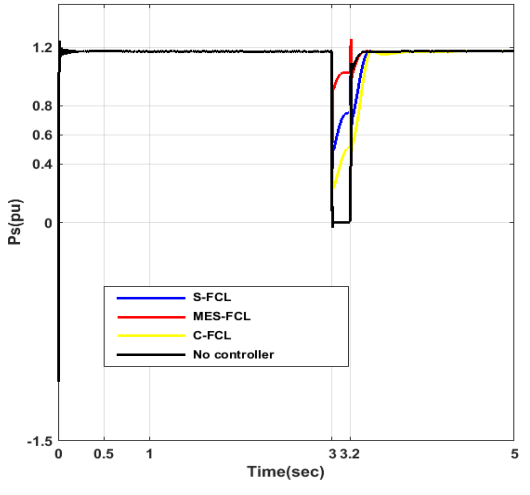

Fig. 23. Active power.

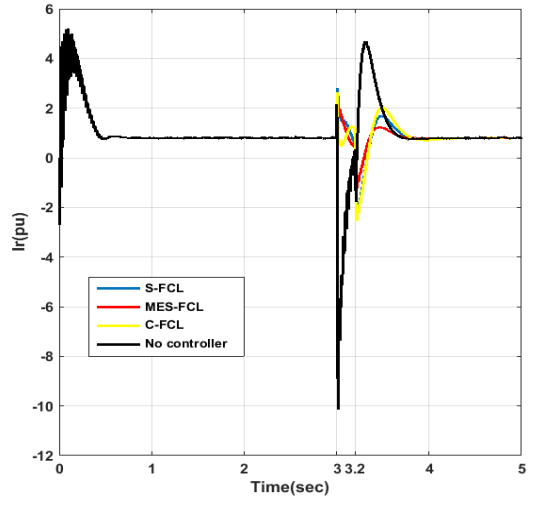

Fig. 24. Rotor current.

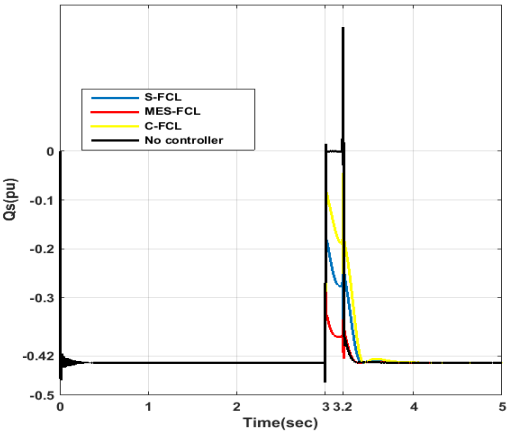

Fig. 25. Reactive power

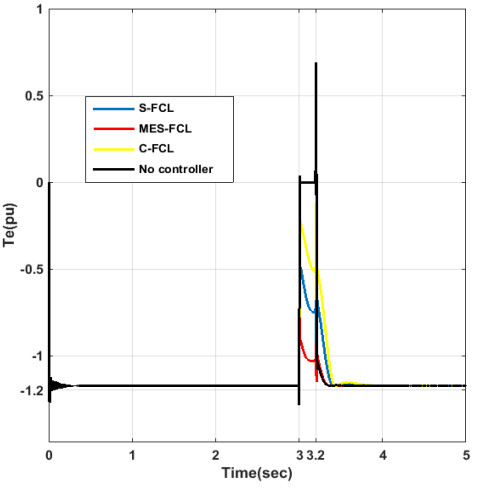

Fig. 26. Electromagnetic torque.

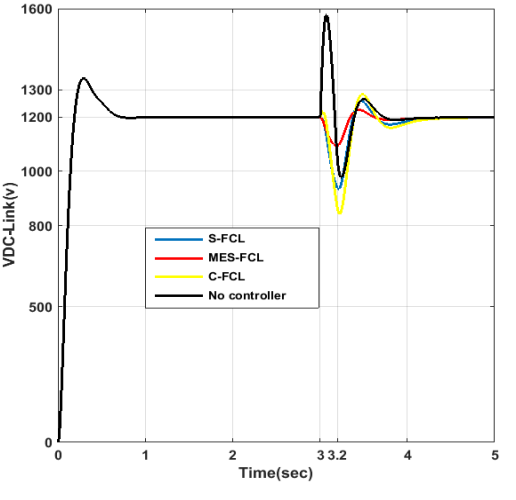

Fig. 27. Voltage DC-Link.

7. CONCLUSION

Under unbalance grid conditions, the negative sequence component of stator voltage leads to the oscillation of power (active-reactive) and electromagnetic torque with twice the grid frequency. The controlling Rotor Side Converter (RSC) aims to eliminate power and torque oscillations. In order to regulate DC-Link voltage, an Extended State Observer (ESO) is employed. In this controlling method, DC-Link voltage was controlled without measuring the GSC current and, due to using a Generalized Proportional-Integral (GPI) controller, the improved dynamic response was resistant against voltage changes, and settling time was reduced. In this paper, a new topology of FCL is proposed to improve the transient stability of DFIG. The effectiveness of the proposed FCL and its performance is compared with C-FCL. Simulation results show that the proposed FCL model is more capable to respond to a fault and return back to the normal state within a shortest possible time. The proposed FCL gives not only lower voltage drop but also speeds up voltage recovery and limits the fault current.

REFRENCES

[1] L. Xu, and Y. Wang, **"Dynamic modeling and control DFIG based wind turbines under unbalance network condition."** *IEEE Transactions on power system.* Vol. 22, pp. 314-323, 2007.

[2] S. M. H. Hosseini, and A. R. Rezvani, (2020, May). Modeling and simulation to optimize direct power control of DFIG invariable-speed pumped-storage power plant using teaching–learning-based optimization techniquetion. Soft Computing (springer), [Online]. Available.

[3] A. Yazdani, and R. Iravan, **"A united dynamic model and control for the voltage-sourced converter under unbalanced grid conditions,"** *IEEE Trans on Power Delivery,* Vol. 21, pp. 1620-1629, 2006.

[4] Y. Wang, and L. Xu, **"Control of DFIG-based wind generation systems under unbalanced network supply,"** *in 2007 Electrical Machines & Drives Conference-IEMDC,* Vol. 7, pp. 430-435.

[5] R. Cardenas, R. Pena, S. Alepuz, and G. Asher, **"Overview of control systems for the operation of DFIGs in wind energy applications,"** *IEEE Trans. Ind. Electron.,* Vol. 60, No. 7, pp. 2776–2798, Jul. 2013.

[6] S. M. H. Hosseini, and M. R. Semsar, **"A Novel Technology for Control of Variable Speed Pumped Storage Power Plant,"** *Journal of Central South University (Springer),* Vol. 23, pp. 2008-2023, August. 2016.

[7] S. M. H. Hosseini, and S. Eslami, **"Modeling of PSPP Control System by Using Vector Control Principle and VSI,"** *in 2019 International Conference on Power Generation System and Renewable Energy Technologies (PGSRET)*.

[8] As. S. Barreto. M. S. Salles. M. B. C. Lira. V. M. Jacomin, and R. V. Filho**, "A direct power control for DFIG under a three- phase symmetrical voltage sag condition",** *Control Engineering Practice,* Vol. 65, pp. 48-58, 2017.

[9] M. J. Zandzadeh, and A. Vahedi, **"Modeling and improvement of direct power control of DFIG under unbalanced grid voltage condition,"** *Electrical power & Energy systems.* Vol. 59, pp. 58-65, 2014.

[10] K. Xiahou, Y. Liu, L. Wang, M. S. Li, and Q. H. Wu, **"Control of DFIG's Rotor-Side Converter With Decoupling of Current Loops Using Observer-Based Fractional-Order Sliding-Mode Regulators,"** *IEEE Access,* Vol. 7, pp. 163412-163420, Nov. 2019.

[11] G. Cai, C. Liu, and D. Yang, **"Rotor current control for a doubly-fed induction generator using a novel nonlinear robust control approach based on extended state observer-backstepping"** *SAGE Transactions of the Institute of Measurement and Control,* Vol. 1, pp. 1-11, July. 2014.

[12] S. Orlando, G. Henrique, M. Antonio, and C. Adriano, **"Nonlinear control of the doubly-fed induction generator in wind power systems,"** *Renewable Energy,* Vol. 35, pp. 1662–1670, 2010.

[13] B. Beltran, T. Ahmed-Ali, and M. E. H. Benbouzid, **"Sliding mode power control of variable-speed wind energy conversion systems,"** *IEEE Transaction on Energy Conversion,* Vol. 23, No. 2, pp. 551–558, Jun. 2008.

[14] B. Beltran, T. Ahmed-Ali, and M. E. H. Benbouzid, **"High-order sliding mode control of variable-speed wind turbines,"** *IEEE Trans. Ind. Electron.,* Vol. 56, No. 9, pp. 3314–3321, Sep. 2009.

[15] A. S. Lock, E. d. Silva. M. E. Elbuluk, and C. B. Jacobina, **"A clamping current control Technique, based on one cycle control OCC,"** *in 2009 IEEE Power Electronics Specialists Conference, Record,* pp. 319–325.

[16] N. Femia, and M. Fortunato, **"Dynamic model of one-cycle control for converters operating in continuous and discontinuous conduction modes,"** *International Journal of Circuit Theory and Applications,* Vol. 37. No. 5, pp. 661–686, 2009.

[17] J. Yang, H. Cui, S. Li, and A. Zolotas, **"Optimized active disturbance rejection control for DC-DC buck converters with uncertainties using a reduced-order GPI observer,"** *IEEE Transactions on Circuits and Systems,* Vol. 65, pp. 832–841, 2018.

[18] J. Lu, S. Golestan, M. Savaghebi, J. C. Vasquez, J. M. Guerrero, and A. Marzabal, **"An enhanced State observer for DC-Link voltage control of three-Phase AC/DC converters,"** *IEEE Transactions on Power Electronics.,* Vol. 33, pp. 936-942, 2018.

[19] G. Zhiqiang, **"Scaling and bandwidth-parameterization based controller tuning,"** *in 2003 American Control Conference.,* Vol. 6, pp. 4989-4996.

[20] Z. Song, C. Xia, and T. Liu, **"Predictive Current Control of Three- Phase Grid-Connected Converters With Constant Switching Frequency for Wind Energy Systems,"** *IEEE Transactions on*

Industrial Electronics, Vol. 60, No. 6, pp. 2451-2464, 2013.

[21] A. Kumar, and J. Lu, "**Enhanced-accuracy augmented state-space approach to steady –state modeling of resonant converters,"** *16 th Workshop on Control and Modeling Power Electronics, IEEE,* 03 Sep. 2015.

[22] M. Malakar, P. Ripat,**"State estimations of DFIG using an Extended Kalman Filter with an augmented state model,"** *in 2015 P Eighteenth National Power System Conference, IEEE,* 11 May.

[23] T. D. Vrionis; X. L. Koutiva, and N. A. Vovos, **"A Genetic Algorithm-Based Low Voltage Ride-Through Control Strategy for Grid Connected Doubly Fed Induction Wind Generators,"** *Power Systems, IEEE Transactions on*, Vol. 29, No. 3, pp. 1325-1334, May. 2014.

[24] D. V. N. Ananth, and G. V. Nagesh Kumar, **"Fault ride-through enhancement using an enhanced field oriented control technique for converters of grid connected DFIG and STATCOM for different types of faults,"** *ISA Transactions*, April. 2015.

[25] V. F. Mendes, and D. E. SOUSA, C. V. Hofmann, Wilfried, **''Doubly-fed induction generator ride-through fault capability using resonant controllers for asymmetrical voltage sags,''** *Renewable Power Generation, IET*, Vol. 9, No 7, p. 783-791, 2015.

[26] J. Yang; J. E. Fletcher, and J. O'Reilly, **"A Series-Dynamic-Resistor-Based Converter Protection Scheme for Doubly-Fed Induction Generator During Various Fault Conditions,"** *Energy Conversion, IEEE Transactions on*, Vol. 25, No. 2, pp. 422-432, June. 2010.

[27] S. A. A. Shahriari, M. Abapour, A. Yazdian, and M. R. Haghifam, **"Minimizing the impact of distributed eneration on distribution protection system by solid state fault current limiter,"** *Transmission and Distribution Conference and Exposition, 2010 IEEE PES*, Vol. 1, No. 7, pp. 19-22, April. 2010.

[28] S. Alaraifi, M. S. El Moursi and H. H. Zeineldin, **"Optimal Allocation of HTS-FCL for Power System Security and Stability Enhancement,"** *Power Systems, IEEE Transactions on*, Vol. 28, No. 4, pp. 4701-4711, Nov. 2013.

[29] H. Radmanesh, S. H. Fathi, G. B. Gharehpetian, and A. Heidary, **"Bridge-Type Solid-State Fault Current Limiter Based on AC/DC Reactor,"** IEEE *Transactions on Power Delivery*, Vol. 31, No. 1, pp. 200-209, Feb. 2016.

[30] M. Nazari-Heris, H. Nourmohamadi, M. Abapour, and M. Sabahi, **"Multilevel Nonsuperconducting Fault Current Limiter: Analysis and Practical Feasibility,"** *IEEE Transactions on Power Electronics*, vol. 32, no. 8, pp. 6059-6068, Aug. 2017.

[31] S. Chen, P. Li, R. Ball, J. F. de Palma, and B. Lehman, **"Analysis of a Switched Impedance Transformer-Type Nonsuperconducting Fault Current Limiter,"** *IEEE Transactions on Power Electronics*, Vol. 30, No. 4, pp. 1925-1936, April. 2015.

[32] M. E. Elshiekh, D. A. Mansour, and A. M. Azmy, **"Improving Fault Ride- Through Capability of DFIG-Based Wind Turbine Using Superconducting Fault Current Limiter,"** *Applied Superconductivity, IEEE Transactions on*, Vol. 23, No. 3, pp. 5601204-5601204, June. 2013.

[33] G. Wenyong, X. Liye, D. Shaotao, L. Yuanhe, X. Xi Z. Wei, and L. Luo, **"LVRT Capability Enhancement of DFIG With Switc Type Fault Current Limiter,"** *Industrial Electronics, IEEE Transactions on*, Vol. 62, No. 1, pp. 332-342, Jan. 2015.

[34] G. Wenyong, X. Liye, D. Shaotao, X. Xi, L. Yuanhe, and W. Yifei, **"Evaluation of the Performance of BTFCLs for Enhancing LVRT Capability of DFIG,"** *Power Electronics, IEEE Transactions on*, Vol. 30, No. 7, pp. 3623-3637, July. 2015.

[35] H. A. Mohammadpour, A. Ghaderi, H. Mohammadpour, **''Low voltage ride-through enhancement of fixed-speed wind farms using series FACTS controllers,''** *Sustainable Energy Technologies and Assessments*, Vol. 9, pp. 12-21, 2015.

[36] C. Sourkounis, and P. Tourou, **"Grid code requirements for wind power integration in Europe,"** *in 2013 Conf. Paper Energy*, Hindawi Publishing Corporation.

[37] M. H. Ali, **"Wind energy systems: solutions for power quality and stabilization,"** Taylor & Francis Group, CRC Press, 1st ed., 2012.

[38] F. Iov, A. D. Hansen, P. E. Sørensen, **"Mapping of grid faults and grid codes,"** Risø National Laboratory, Technical University of Denmark, 2007.